PERGAMON

International Journal of Heat and Mass Transfer 42 (1999) 275–286

International Journal of HEAT and MASS TRANSFER

Thermal performance of a latent heat energy storage ventilated panel for electric load management

A. Laouadi†, M. Lacroix*

Groupe THERMAUS, Departement de Génie Mécanique, Université de Sherbrooke, Sherbrooke, Québec, Canada, J1K 2R1

Received 29 April 1997; in final form 18 March 1998

Abstract

A theoretical study was conducted to assess the thermal performance of a ventilated panel heating unit. The unit employs the latent heat energy storage method to level the electrical energy demand for domestic space heating during peak hours. A one-dimensional, semi-empirical model was developed to predict the dynamic thermal behavior of the storage unit under cyclic melting and solidification. The results show that the storage unit may be charged and discharged more than twice a day with a charge time shorter than the discharge time. The temperature of the plate in contact with the ambient air may be controlled to reach higher values without compromising the unit heating power. General correlations of the charge and discharge times are established for a wide range of the governing parameters.

Nomenclature

a, b exponents, equation (27)
a_p, a_{nb} discretization coefficients, equation (16)
A plate surface area
A_0, A_1, A_2, constants, equation (22)
c specific heat, or charge time constant [equation (27)]
C_w, c_w equivalent thermal conductivity coefficients, equation (15)
d discharge time constant, equation (27)
E supplied electric power per unit area [W m^{-2}]
E_0 threshold of the supplied electric power per unit area, equation (26)
f local liquid fraction
h_{ci}, h_{ce} inside and outside convection coefficients, respectively
h_e sum of the outside radiation and convection coefficients
h_{ri}, h_{re} inside and outside radiation coefficients, respectively, equation (13)
h_t $(=h_e+h_{ci}+h_{ri})$
k thermal conductivity
k_{eff} effective thermal conductivity of the mixture
k_{eq} equivalent thermal conductivity of the melt, equation (15)
l PCM thickness
l_0 spacing between plates P2 and P3
L plate length
m, n exponents in equation (15) or in equation (27)
M air mass flow rate [kg s^{-1}]
NTU number of thermal units $(2Ah_{ci}/Mc_f)$
NTU_0 value of NTU corresponding to $T_{P3}=T_s$, equation (23)
NTU_1 value of NTU corresponding to $\eta_{P3}=\eta_f$, equation (25)
Nu Nusselt number
q_f heat per unit area removed by the ventilating air, equation (20)
q_{P2} total heat per unit area transferred to the environment through plate P2, equation (19)
q_{P3} heat per unit area removed by plate P3
Ra_l Rayleigh number for the PCM $(g\beta\,(T_{P1}-T_m)l^3/\alpha\nu)$
S PCM liquid thickness
t time
t_c, t_d charge and discharge times, respectively
T temperature

* Corresponding author. E-mail: marcel.lacroix@gme.usherb.ca

† Currently holding an NSERC fellowship at the National Research Council Canada, Institute For Research in Construction, Montreal Road, Ottawa, Ontario, Canada K1A 0R6.

0017–9310/98 $19.00
PII: S0017–9310(98)00121–5

T^* dimensionless temperature $\{(T-\bar{T}_p)/(T_a-\bar{T}_p)\}$
T_a ambient temperature
T_f bulk temperature of the ventilating air
$\bar{T}_f$ average of the air bulk temperature over the plate length
T_m average fusion temperature
T_{P1} temperature of plate P1
T_{P2} temperature of plate P2
T_{P3} temperature of plate P3
T_s ventilating air temperature at the outlet
$\bar{T}_P$ average temperature of plates P1 and P2, $\{=(T_{P2}+T_{P3})/2\}$
T_1, T_2 lower and upper temperatures of the melting range, respectively
x, y space variables.

Greek symbols
α thermal diffusivity of the wax
β thermal expansion coefficient of the wax
δH enthalpy difference between the liquid and the solid phases, equation (3)
ΔH latent heat of fusion
Δt time increment
ΔT melting range (T_2-T_1)
Δx control volume width
ε_{P2} emissivity of plate P2
ε^i_{P3} interior surface emissivity of plate P3
ε^e_{P3} exterior surface emissivity of plate P3
η_f, η_{P3} heat removal fractions of the ventilating air and plate P3, respectively
μ dynamic viscosity of the wax
ν cinematic viscosity of the wax (μ/ρ)
ρ density
σ Stephan–Boltzmann constant of radiation.

Subscripts
f ventilating air
l liquid
m mixture
s solid.

1. Introduction

In northern countries, electrical energy consumption for domestic space heating represents a high percentage of the total consumption. During harsh winter days, electrical energy demand is particularly acute in the morning and late in the evening. As a result, quite often, the distribution grid is overloaded resulting in costly power failures. This severe problem has created the need to shift some of the on-peak demand to the off-peak periods by making use of electrical storage systems. In these systems, electrical energy is converted to thermal energy by passing heat wires through the storage material. Heat is then stored for a period of time, usually during the night, and subsequently used the next morning. During on-peak periods, the current is automatically disconnected and the unit discharges its heat to the living space by radiation and/or convection (natural and/or forced). The unit may be designed to produce enough heat during the off-peak hours to maintain a comfortable temperature in the living space and at the same time to store enough heat to meet the on-peak requirements. A good understanding of the cyclic heat transfer process involved is therefore essential for predicting accurately the thermal performance of the system and for avoiding costly system overdesign.

Electrical energy may be stored in the form of sensible heat using high thermal capacity materials at high temperatures as well as in the form of latent heat using phase change materials (PCMs). The advantages of the latter form are well recognised. Extensive work has been carried out in the field of solar and thermal energy storage using PCMs. Different Heat exchanger configurations to store and recover heat have been studied [1–8]. Cao and Faghri [9, 10] numerically simulated the thermal performance a shell-and-tube heat exchanger employing a low Prandtl number transporting fluid for space application. The transient flow momentum and energy equations were solved in tandem with the tube's wall and PCM energy equations. They concluded that using a steady full developed heat transfer correlation to calculate the heat transfer coefficient inside the tube would introduce significant errors in the results. Bellicci and Conti [11, 12] numerically studied a solar receiving, shell-and-tube heat exchanger, similar to that modelled by Cao and Faghri [9]. They treated the flow inside the tube as steady fully developed, and employed standard correlations to calculate the heat transfer coefficient. Recently, Zhang and Faghri [13] developed a semi-analytical model for the shell-and-tube heat exchanger studied by Cao and Faghri [9]. They used a one-dimensional integral method to solve the PCM energy equation, and treated the flow inside the tube as steady thermally developing with constant velocity profile. Zhang and Faghri [13] concluded that the laminar forced flow inside the tube never reached the thermally developed state. The Nusselt number of the flow varies with time, and is bound by the Nusselt numbers for the constant heat flux (CHF) and uniform wall temperature (UWT) boundary conditions.

Cyclic charge and discharge of latent heat energy storage systems have received increasing attention in the literature. Kalhori and Ramadhyani [14] conducted experiments on cyclic melting and freezing around finned and unfinned vertical cylinders embedded in a PCM. Jariwala et al. [15] dealt with cyclic melting and freezing around a helical tube embedded in a PCM. Hasan et al. [16] carried out experimental and analytical studies on cyclic charge and discharge of latent energy in a planar slab. Recently, Gong et al. [17] presented a parametric study on cyclic melting and freezing in composite PCM slabs using finite elements method. PCMs with different melting temperatures were used.

However, storage of electrical energy using phase change materials (PCMs) has received very little attention in the literature. Farid and Husian [18] developed a storage heater utilising off-peak electricity. It consists of multi-units filled with a paraffin wax and arranged in a vertical rectangular container. During the charge cycle, heat is supplied to the units using an electrical heater fixed at the center axis of each unit. During the discharge cycle, heat is recovered by circulating air through the spaces between the units.

The objectives of the present paper are:

(1) To develop a model for a ventilated heating panel unit that uses latent heat energy storage to shift the electrical energy demand from on-peak periods to off-peak periods.
(2) To predict the thermal performance of the storage unit under cyclic charge and discharge modes.
(3) To control the panel temperature, which may reach high values at high charging heating powers.

Storage of electrical energy in the form of latent heat energy during the off-peak periods is very important for electrical energy cost saving.

2. Mathematical formulation

A schematic representation of the storage unit is depicted in Fig. 1. The unit consists of three spaced parallel plates (P1, P2 and P3). The PCM fills the space between plates P1 and P2 while ambient air can be forced to flow through the space between plates P2 and P3. Plate P1 is insulated from the surroundings and heated during the charge period using electrical elements whilst plate P3 allows heat exchange with the environment by natural convection and radiation. On the other hand, Plate P2 exchanges heat by forced convection with the adjacent air and by radiation with plate P3. The unit may be positioned vertically (attached to a wall) or horizontally (attached to a ceiling) with the insulated plate at the top. The unit may be charged and discharged several times a day. During the charge period, the unit is heated until the temperature of plate P2 reaches a higher set point temperature (T_{high}) so that the liquid PCM becomes superheated. At this point the electric current is shut off and the unit starts releasing its heat to the surroundings until the temperature of plate P1 reaches a lower set point temperature (T_{low}) and all the PCM becomes a subcooled solid. Soon after, the next charge period starts, and so on for the subsequent discharge and charge cycles.

The mathematical description of the problem relies on the following assumptions:

(1) The phase change is one-dimensional and conduction dominated. Convection in the melt may, however, be accounted for by defining an equivalent thermal conductivity of the liquid phase [18].
(2) Airflow between plates P2 and P3 is fully developed with negligible heat storage. The bulk air temperature may vary along the plate.

Assumption 1 stems from the fact that the small PCM thickness and the low PCM thermal conductivity are the main controlling parameters for the heat transfer. Deviation of the model may, however, result at the end of the melting stage where natural convection is the dominant mode. In this case, using a variable equivalent thermal conductivity of the melt will satisfy the global heat balance of the unit and will, consequently, result in averaged temperatures.

Subjected to the foregoing assumptions, the governing heat transfer equations for the PCM and for the air take the following forms [19, 20]:

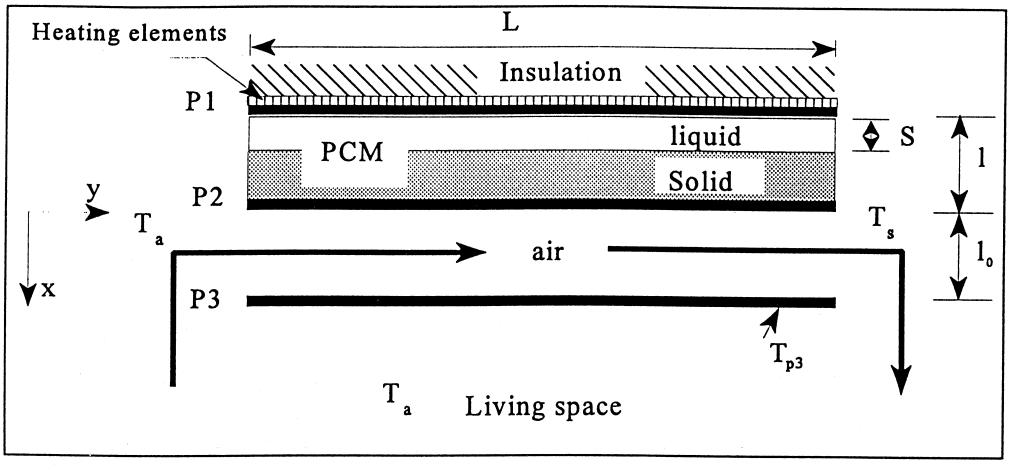

Fig. 1. Schematic representation of the storage unit.

$$(\rho c)_{\mathrm{m}}\frac{\partial T}{\partial t}=\frac{\partial}{\partial x}\left(k_{\mathrm{eff}}\frac{\partial T}{\partial x}\right)-\delta H\frac{\partial f}{\partial t} \tag{1}$$

$$Mc_{\mathrm{f}}\frac{\mathrm{d}T_{\mathrm{f}}}{\mathrm{d}y}=(2h_{ci}\mathrm{A}/\mathrm{L})(\bar{\mathrm{T}}_{\mathrm{P}}-\mathrm{T}_{\mathrm{f}}) \tag{2}$$

where δH is the enthalpy difference between the liquid and the solid phases present at the same temperature within the melting range. It is given by:

$$\delta H=\rho_{\mathrm{l}}(\Delta H)+\int_{T_2}^{T}(\rho c)_{\mathrm{l}}\,\mathrm{d}T-\int_{T_1}^{T}(\rho c)_{\mathrm{s}}\,\mathrm{d}T \tag{3}$$

k_{eff} is the effective thermal conductivity of the mixture, ρ the density, c the specific heat, ΔH the latent heat of fusion, f the local liquid fraction, M the air mass flow rate, h_{ci} the convection coefficient of the ventilating air, A the plate surface area, L the plate length, $(\rho c)_{\mathrm{m}}$ the mixture thermal capacity, T_{f} the bulk air temperature, $\bar{T}_{\mathrm{P}}=(T_{\mathrm{P2}}+T_{\mathrm{P3}})/2$, and T_1 and T_2 the lower and upper temperatures of the melting range (ΔT), respectively. The local liquid fraction takes the following values:

$$f=\begin{cases}0: & T\leqslant T_1\\ [T-T_1]/\Delta T: & T_1<T<T_2\\ 1: & T\geqslant T_2\end{cases}. \tag{4}$$

The corresponding initial and boundary conditions are as follows:

$$t=0:\quad T=T_{\mathrm{f}}=T_{\mathrm{a}} \tag{5}$$

$$x=0:\quad -k_{\mathrm{eff}}\frac{\partial T}{\partial x}=\begin{cases}E, & \text{for the charge period}\\ 0, & \text{for the discharge period}\end{cases} \tag{6}$$

$$x=l:\quad -k_{\mathrm{eff}}\frac{\partial T}{\partial x}=q_{\mathrm{P2}} \tag{7}$$

$$y=0:\quad T_{\mathrm{f}}=T_{\mathrm{a}} \tag{8}$$

where E is the electric power per unit area, and q_{P2} the total heat per unit area transferred by plate P2 to the environment. Equation (2) admits an exact solution of the form:

$$T_{\mathrm{f}}^{*}=\frac{T_{\mathrm{f}}-\bar{T}_{\mathrm{P}}}{T_{\mathrm{a}}-\bar{T}_{\mathrm{P}}}=\mathrm{e}^{-NTU\cdot(Y/L)} \tag{9}$$

where $NTU=2Ah_{\mathrm{ci}}/\mathrm{Mc_f}$ is the number of thermal units. The average bulk air temperature over the plate length is given by:

$$\bar{T}_{\mathrm{f}}^{*}=\frac{\bar{T}_{\mathrm{f}}-\bar{T}_{\mathrm{P}}}{T_{\mathrm{a}}-\bar{T}_{\mathrm{P}}}=[1-\mathrm{e}^{-NTU}]/NTU. \tag{10}$$

The temperature of plate P3 is expressed as:

$$T_{\mathrm{P3}}=\frac{h_{\mathrm{ri}}T_{\mathrm{P2}}+h_{\mathrm{ci}}\bar{T}_{\mathrm{f}}+h_{\mathrm{e}}T_{\mathrm{a}}}{h_{\mathrm{ri}}+h_{\mathrm{ci}}+h_{\mathrm{e}}} \tag{11}$$

and in dimensionless form:

$$T_{\mathrm{P3}}^{*}=\frac{T_{\mathrm{P3}}-\bar{T}_{\mathrm{P}}}{T_{\mathrm{a}}-\bar{T}_{\mathrm{P}}}=\frac{1}{h_{\mathrm{ri}}+h_{\mathrm{ci}}+h_{\mathrm{e}}}\{h_{\mathrm{e}}+h_{\mathrm{ci}}(1-\mathrm{e}^{-NTU})/NTU\} \tag{12}$$

where h_{ri} is the inside radiation coefficient and h_{e} is the sum of the outside radiation and convection coefficients ($h_{\mathrm{re}}, h_{\mathrm{ce}}$). The radiation coefficients ($h_{\mathrm{ri}}, h_{\mathrm{re}}$) are given by:

$$h_{\mathrm{ri}}\approx\frac{4\sigma}{1/\varepsilon_{\mathrm{P2}}+1/\varepsilon_{\mathrm{P3}}^{\mathrm{i}}-1}\bar{T}_{\mathrm{P}}^{3};\quad h_{\mathrm{re}}=\varepsilon_{\mathrm{P3}}^{\mathrm{e}}\sigma[T_{\mathrm{a}}^{2}+T_{\mathrm{P3}}^{2}]\cdot[T_{\mathrm{a}}+T_{\mathrm{P3}}]. \tag{13}$$

The inside and outside convection coefficients h_{ci} and h_{ce} are given by correlations.

To account for the effect of natural convection in the melt, the thermal conductivity of the liquid phase is replaced by an equivalent conductivity, which may be estimated by the following formulae:

$$\frac{k_{\mathrm{eq}}}{k_1}=\frac{Nu_{\mathrm{conv}}}{Nu_{\mathrm{cond}}}=\frac{c_{\mathrm{w}}Ra_{\mathrm{l}}^{n}}{[l\cdot\partial T/\partial x]/[T_{\mathrm{m}}-T_{\mathrm{P1}}]} \tag{14}$$

where Nu_{conv} and Nu_{cond} stand for the Nusselt numbers in the presence and absence of free convection in the melt, respectively. The former is often determined by correlations which involve the constants c_{w} and n. Ra_{l} is the Rayleigh number and $T_{\mathrm{m}}=(T_2+T_1)/2$ is the average melting temperature. Assuming that the melting process is quasi-steady, the temperature gradient in the melt $\partial T/\partial x$ may be approximated by $(T_{\mathrm{m}}-T_{\mathrm{P1}})/S$; where S is the PCM liquid thickness. Equation (14) then becomes:

$$\frac{k_{\mathrm{eq}}}{k_1}=c_{\mathrm{w}}Ra_{\mathrm{l}}^{n}(S/l)\equiv C_{\mathrm{w}}Ra_{\mathrm{l}}^{n}(S/l)^{m} \tag{15}$$

Farid and Kanzawa [4], Hirata and Nishida [21] and Lacroix [8] have successfully used this correlation. C_{w}, m and n are constants to be determined experimentally.

3. Numerical model

Since there is no exact solution for the phase change problem under study, a numerical procedure, based on the control volume approach combined with an implicit scheme, was used to solve for the temperature in the PCM. The discretized form of equation (1) for a node P leads to:

$$a_{\mathrm{P}}T_{\mathrm{P}}=\Sigma\,a_{\mathrm{nb}}T_{\mathrm{nb}}+\delta H(f_{\mathrm{P}}^{0}-f_{\mathrm{P}})(\Delta x_{\mathrm{P}}/\Delta t)+(\rho c)_{\mathrm{m}}(\Delta x_{\mathrm{P}}/\Delta t)T_{\mathrm{P}}^{0} \tag{16}$$

where a_{P} and a_{nb} are the coefficients for the node P and

its neighbors, respectively. Δx_P is the width of the control volume associated with the node P and the superscript 0 stands for values at the previous time step. Equation (16) is non-linear and involves two unknown variables T and f. The liquid fraction is determined by the following iterative procedure:

(1) For a given value f^k at iteration k, equation (16) is solved for the temperature T_P^k.
(2) The liquid fraction is updated for the next iteration $(k+1)$ using the following formulae [19, 20]:

$$f_P^{k+1} = \frac{\delta H/(\rho c)_m}{\delta H/(\rho c)_m + \Delta T} f_P^k + \frac{T_P^k - T_l}{\delta H/(\rho c)_m + \Delta T}. \quad (17)$$

Equation (17) is applied to each node in conjunction with the over/undershoot correction:

$$f_P^{k+1} = 0 \quad \text{if } f_P^{k+1} < 0 \quad \text{and} \quad f_P^{k+1} = 1 \quad \text{if } f_P^{k+1} > 1. \quad (18)$$

(3) The corresponding temperature T_P^{k+1} is obtained from equation (16).
(4) Steps (2) and (3) are repeated until convergence is reached.

Equation (17) may be overrelaxed with a relaxation coefficient ω $(1 \leqslant \omega \leqslant 2)$ to accelerate convergence. Convergence is declared when the residual of equation (16) is less than 10^{-2}. This procedure converges in all times, and it is valid for isothermal phase change $(\Delta T = 0)$ as well as for non-isothermal phase change [19, 20].

4. Heat transfer to the environment

It is of practical interest to know the amount of heat transferred to the environment by the ventilating air and by plate P3. The total heat per unit surface area removed by plate P2 to the environment is expressed as:

$$q_{P2} = h_{ci}(T_{P2} - \bar{T}_f) + h_{ri}(T_{P2} - T_{P3}) = (Mc_f/A)(T_s - T_a) + h_e(T_{P3} - T_a). \quad (19)$$

A portion of this heat is evacuated by forced convection by the ventilating air, which reads as:

$$q_f = 2h_{ci}(\bar{T}_P - \bar{T}_f) = (Mc_f/A)(T_s - T_a) \quad (20)$$

and the remaining heat, $q_{P3} = q_{P2} - q_f$, is removed by radiation and natural convection through plate P3.

The fraction of the heat removed by the ventilating air is:

$$\eta_f = \frac{q_f}{q_{P2}} = \frac{A_0(1 - e^{-NTU})}{A_1 NTU + A_2(1 - e^{-NTU})} \quad (21)$$

where the constants A_0, A_1 and A_2 are given by:

$$A_0 = 2h_{ci}(h_t + h_{ri}); \quad A_1 = h_e(h_{ci} + 2h_{ri}); \quad (22)$$

$$A_2 = h_{ci}(h_t + h_{ci} + 3h_{ri}) \quad (22)$$

with $h_t = h_{ci} + h_e$. The fraction of the heat removed by plate P3 is $\eta_{P3} = 1 - \eta_f$.

The dimensionless temperature of the ventilating air at the outlet (T_s^*) and that of plate P3 (T_{P3}^*) and the heat removal fractions (η_f, η_{P3}) are function of NTU and the exchange coefficients h_{ci}, h_{ri} and h_e. This dependency allows better control of the rate of heat transfer to the environment and of the operating temperatures (T_s, T_{P3}) according to the values of the air mass flow rate M (or NTU), the distance l_0 between plates P2 and P3 (or h_{ci}), and the emissivities of plates P2 and P3 (or h_{ri}, h_{re}). According to the values of these parameters, in particular the parameter NTU, the ventilating air temperature at the outlet may be higher or lower than the temperature of plate P3.

Figure 2 shows the profiles of the dimensionless temperatures T_s^* and T_{P3}^* as a function of NTU with h_{ci} and h_{ri} as parameters. The dimensionless temperature T_s^* decreases rapidly with the increase in NTU. The ventilating air exits at the ambient temperature when NTU is very low while it exits at the mean temperature $\bar{T}_P$ when NTU is very large. However, the dimensionless temperature T_{P3}^* decreases slowly and is always bound by the values $(h_t - h_{ri})/(h_t + h_{ri})$ and $h_e/(h_t + h_{ri})$ when NTU varies from a low value to a large value. The curves of T_s^* and T_{P3}^* meet at $NTU = NTU_0$, which is given by the following equation:

$$(h_t + h_{ri})\, e^{-NTU_0} = h_e + h_{ci}(1 - e^{-NTU_0})/NTU_0 \quad (23)$$

The value NTU_0 designates the following operating regimes:

(1) $NTU < NTU_0$. The ventilating air exits at a temperature lower than that of plate P3, $(T_s < T_{P3})$, and

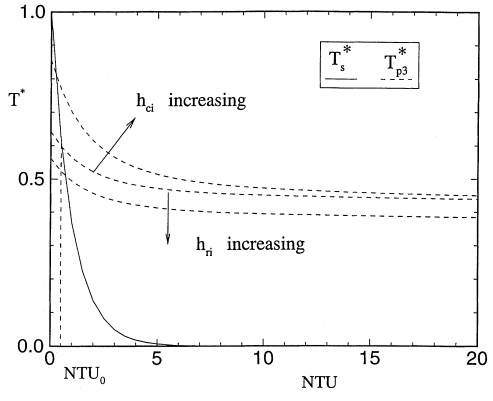

Fig. 2. Profiles of the dimensionless temperatures T_s^* and T_{P3}^* as a function of NTU, h_{ci} and h_{ri}.

the heat is removed from the PCM mostly by the ventilating air.

(2) $NTU > NTU_0$. The ventilating air exits at a temperature higher than that of plate P3, ($T_s > T_{P3}$), and the heat may be removed from the PCM mostly by plate P3, especially at low values of the mass flow rate.

The dimensionless temperature of the ventilating air at the outlet $T_s^*$is controlled only by the number NTU while that of plate P3 is very sensitive to the variations of the plate emissivities, the distance between plates P2 and P3 and the mass flow rate (M). The temperature of plate P3 and the threshold NTU_0 decrease as the convection (h_{ci}) increases while the inverse trend occurs when the radiation coefficient (h_{ri}) increases.

Figure 3 shows the profiles of the heat removal fractions of the ventilating air and of plate P3 as a function of NTU with h_{ri} and h_{ci} as parameters. The heat removal fraction η_f decreases as NTU increases and, consequently, η_{P3} increases. For the extreme values of NTU, one obtains:

$$NTU = 0: \quad \eta_f = \frac{2h_{ci}(h_t + h_{ri})}{h_e(h_{ci} + 2h_{ri}) + h_{ci}(h_t + h_{ci} + 3h_{ri})}$$

$$NTU \to \infty: \quad \eta_f \to 0. \tag{24}$$

Heat is removed mostly by the ventilating air at low values of NTU while it is removed by plate P3 at large values of NTU. The heat removed by the ventilating air is high when the coefficient h_{ci} is high whilst the inverse trend happens to the heat removed by plate P3. However, increasing the radiation coefficient h_{ri} will result in a lower heat removal fraction of the ventilating air and a higher heat removal fraction of plate P3. At equal heat removal fractions, $\eta_f = \eta_{P3} = 0.5$, the corresponding NTU_1 is given by the following equation:

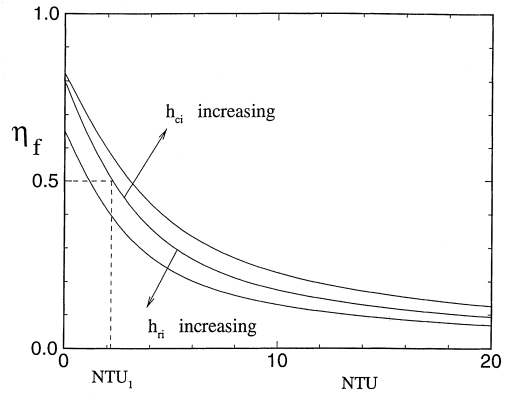

Fig. 3. Profile of the heat removal fraction η_f as a function of NTU, h_{ci} and h_{ri}.

$$\frac{1 - e^{-NTU_1}}{NTU_1} = \frac{h_e}{h_{ci}} \cdot \frac{2h_{ri} + h_{ci}}{4h_{ri} + 2h_{ci} + 3h_e}. \tag{25}$$

5. Experimental apparatus and validation

The foregoing mathematical model was validated with experimental data. To achieve this goal, an experimental storage unit was constructed, and experiments were performed. A layout of the storage unit is shown in Fig. 4. The unit consists of two parallel copper plates (P1, P2), 1.6 mm thick, 380 mm wide and 300 mm long, mounted 20 mm apart. The space between the plates is filled with Sunoco wax P116, a commercial paraffin. Heating strips are uniformly distributed on plate P1, which is insulated with a 80 mm thick fiberglass layer while plate P2 allows heat exchange with the surroundings by radiation and free convection. The outside surface of plate P2 is painted black with an emissivity of 0.98. The entire planar unit is supported by a wooden frame and it may be oriented vertically or horizontally. The unit is positioned at height of 950 mm above the floor. Thirty copper-constant thermocouples, embedded in the PCM, are deployed on five rows 50 mm apart and their positions are indicated by the letters A, B, C, D and E in Fig. 4. Each row contains five thermocouples spaced 4 mm apart. Another thermocouple is used to measure the ambient temperature. All thermocouples are calibrated with an uncertainty of ± 0.5°C and connected to a data acquisition system. During the storage period, an on/off electric source supplies constant power to the unit. The electric source is turned on when the temperature of plate P1 reaches the lower set point. Once the PCM is completely melted and the temperature of the plate P2 reaches the higher set point, the electric source is disconnected and the unit discharges its heat to the surroundings until the PCM has resolidified. Control of the charge and discharge periods is ensured using an automatic on/off relay. The electric power is measured by a Wattmeter device with an uncertainty of ± 2 W. The readings of the thermocouples are collected every second, averaged every ten minutes and then stored every 400 seconds. For a typical experiment, the melting and resolidification cycles are repeated several times uninterrupted for a few days.

The physical properties of the wax P116 reported by the manufacturer are $T_f = 47$°C, $L = 225$ kJ kg^{-1}, $\rho_s = 830$ kg m^{-3}, $\rho_l = 773$ kg m^{-3}, $c_s = 2.4$ kJ kg^{-1} K^{-1}, $c_l = 1.9$ kJ kg^{-1} K^{-1}, $k_s = k_l = 0.24$ W m^{-1} K^{-1}, and $\mu = 1.9\ 10^{-3}$ kg ms^{-1} s^{-1}. Figure 5 shows the temporal variation of the measured and predicted temperatures of the plates for a horizontally and vertically oriented unit, respectively. The lower and higher set points for the 120 W ($E = 1053$ W m^{-2}) electric source were fixed at 35 and 50°C, respectively. The numerical simulations were carried out with a space increment $\Delta x = 2$ mm and a

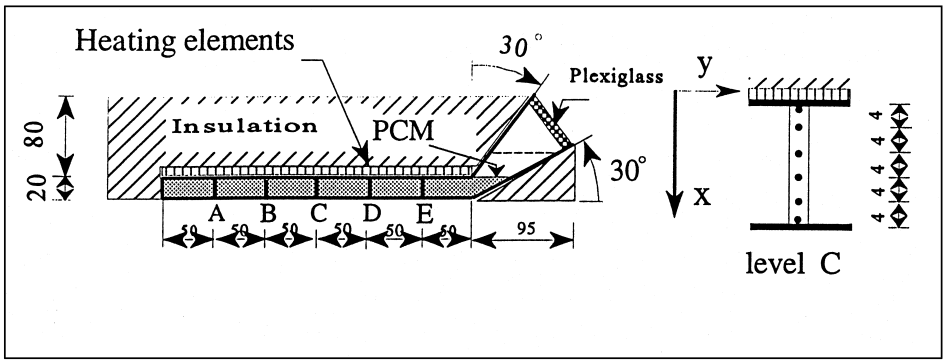

Fig. 4. Cross-section view of the tested storage unit.

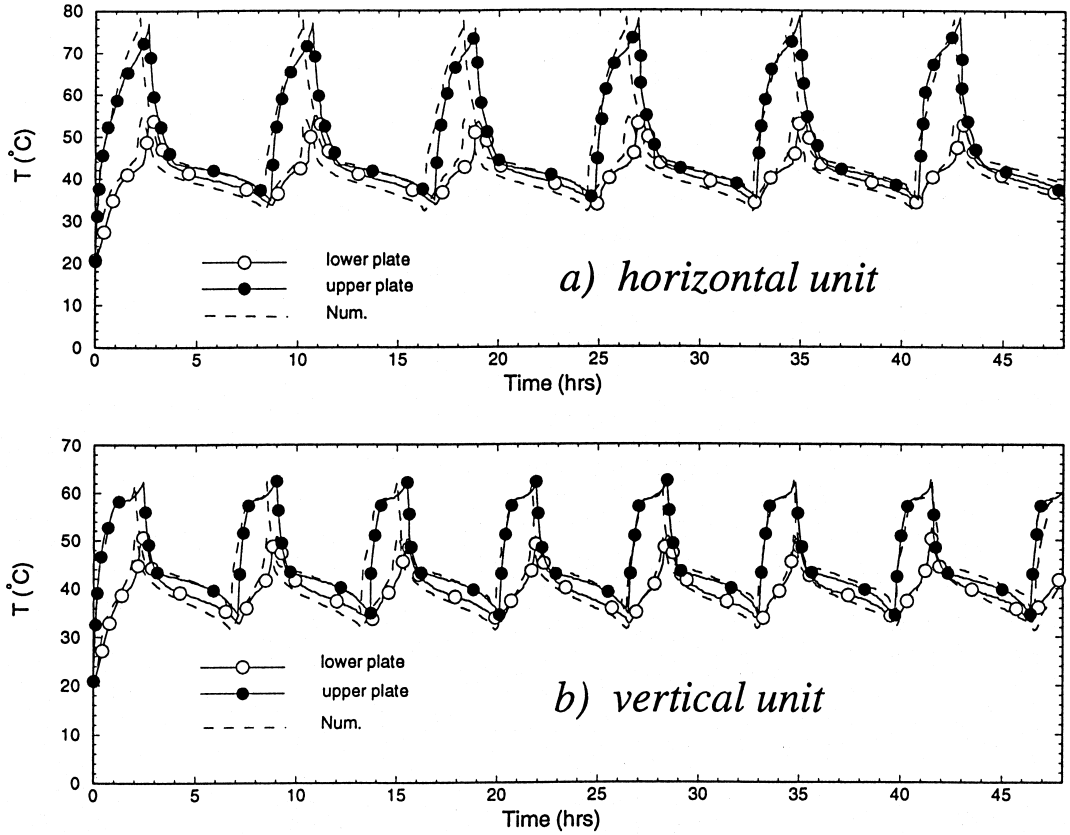

Fig. 5. Cyclic profile of the plate temperatures at level C for $E = 1053$ W m^{-2} and $T_a = 21.2$°C.

time increment $\Delta t = 400$ s. The constants in correlation (15) were estimated by comparing the experimental and numerical results and were found to be $C_w = 0.05$ and $m = 0.65$ for the horizontal unit, and $C_w = 0.12$ and $m = 1$ for the vertical unit. The exponent n was fixed at 0.25 for both positions [4, 8, 21]. The process of melting–freezing is constrained in the range 40–45°C. More details of the experimental validation may be found in Laouadi [19].

6. Results and discussion

A different paraffin wax was used for the numerical study. Its selection was based mainly on its fusion tem-

perature and its well-known thermal properties. However, the selection of a PCM should be based on many criteria, namely, its thermal properties, its interaction with the container and the type of application. A summary of available PCMs is presented in Abhat [22]. The physical properties of the studied PCM were taken from Farid and Husian [18], and are: $k_s = 0.29$ W m^{-1} K^{-1}, $k_l = 0.21$ W m^{-1} K^{-1}, $\rho_s = 910$ kg m^{-3}, $\rho_l = 822$ kg m^{-3}, $c_s = c_l = 1770$ J kg^{-1} K^{-1}, $T_m = 56°C$, $\Delta H = 195$ kJ kg^{-1} and the viscosity $\mu = 0.012$ kg m^{-1} s^{-1}. The wax was cycled around the fusion temperature between the set points $T_{low} = 50°C$ and $T_{high} = 60°C$ to ensure complete melting and solidification at the end of the charge and discharge cycles, respectively, and to minimize the storage of sensible heat in the PCM mass. The ambient temperature T_a was fixed at 21°C for all the simulations. Numerical simulations were carried out with 15 nodes in the x-direction and a time increment $\Delta t = 150$ s. Finer grid sizes and shorter time steps were also used, but the predicted results did not show perceptible difference with the present ones. The convection coefficient h_{ci} is taken from Shah and Bhatti [23], and equal to $2\,k_f/l_0$ for a fully developed laminar flow. The outside convection coefficient h_{ce} was estimated by correlations from Incropera and De Witt [24], and is a function of the Rayleigh number of the ambient air.

Figures 6–9 show the temporal variation of the temperature of the plates and of the ventilating air for the horizontal and vertical units and for two values of NTU (0.4 and 4) situated around the threshold $NTU_0 \approx 0.85$. The spacings l and l_0 are fixed at 0.02 and 0.01 m, respectively, while the plate emissivities are all unity. The supplied electric power is fixed at $E = 700$ W m^{-2}. These figures show that there are two operating regimes. In the first regime ($NTU = 0.4$), the ventilating air exits from the unit at a temperature lower than that of plate P3 (Figs 6 and 7). In the second regime ($NTU = 4$) the inverse

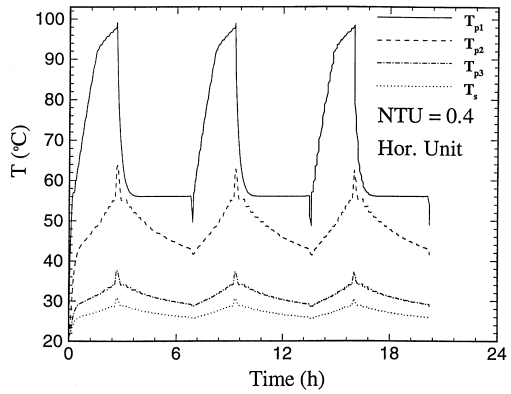

Fig. 6. Temperature time histories of plates P1, P2 and P3 and of the outlet air for $NTU = 0.4$, $E = 700$ W m^{-2}, $l = 0.02$ m, $l_0 = 0.01$ m and $\varepsilon_{P1} = \varepsilon_{P2} = \varepsilon^{i}_{P3} = \varepsilon^{e}_{P3} = 1$ (horizontal unit).

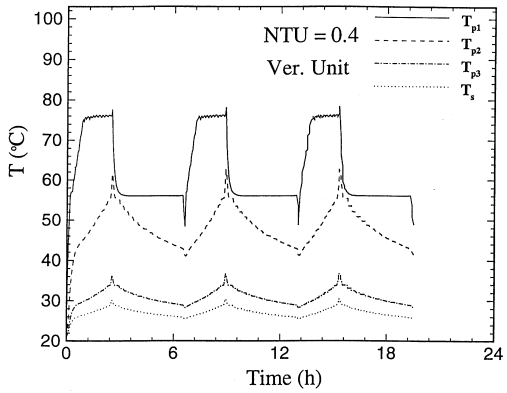

Fig. 7. Temperature time histories of plates P1, P2 and P3 and of the outlet air for $NTU = 0.4$, $E = 700$ W m^{-2}, $l = 0.02$, $l_0 = 0.01$ m and $\varepsilon_{P1} = \varepsilon_{P2} = \varepsilon^{i}_{P3} = \varepsilon^{e}_{P3} = 1$ (vertical unit).

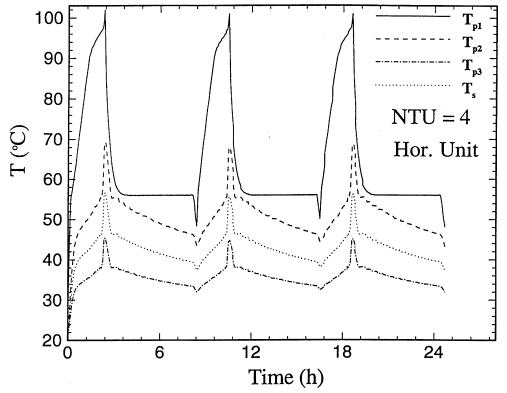

Fig. 8. Temperature time histories of plates P1, P2 and P3 and of the outlet air for $NTU = 4$, $E = 700$ W m^{-2}, $l = 0.02$ m, $l_0 = 0.01$ m and $\varepsilon_{P1} = \varepsilon_{P2} = \varepsilon^{i}_{P3} = \varepsilon^{e}_{P3} = 1$ (horizontal unit).

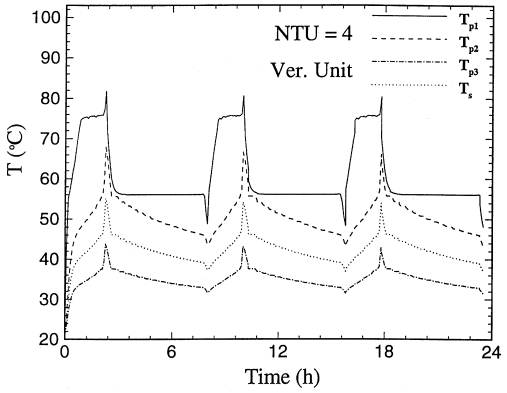

Fig. 9. Temperature histories of plates P1, P2 and P3 and of the outlet air for $NTU = 4$, $E = 700$ W m^{-2}, $l = 0.02$ m, $l_0 = 0.01$ m and $\varepsilon_{P1} = \varepsilon_{P2} = \varepsilon^{i}_{P3} = \varepsilon^{e}_{P3} = 1$ (vertical unit).

trend occurs (Figs 8 and 9). Furthermore, in the first regime heat is removed basically by the ventilating air ($\eta_f = 0.67$) while in the second regime more heat is removed by plate P3 ($\eta_{P3} = 0.32$). If plate P3 were removed from the unit, that is the unit discharges its heat through plate P2, the temperature of the latter would be more than 15°C higher than that of plate P3. The temperatures T_{P3} and T_{P2} vary quite uniformly during the charge and discharge cycles. As a result, the discharge power delivered by the unit to the living space stays somewhat uniform during the whole cycle, except when the molten PCM is superheated. The charge time is less sensitive to the increase in NTU while the discharge time increases considerably.

Figures 6–9 also reveal that the temperature near the heat source increases rapidly as heat is being stored. On the other hand, during the discharge period, this temperature decreases quickly as sensible heat is being released and then it levels out as latent heat is being recovered. As expected, natural convection in the melt is more vigorous when the unit is in the vertical position (Figs 8 and 9) and, consequently, the maximum temperature in the melt is significantly reduced. Free convection in the melt contributes to decrease the charge time while free convection in the ambient air does the inverse. These effects are balanced and, as a result, the charge time is almost the same for the horizontal and vertical units. However, the discharge time is quite shorter when the unit is vertical. The periodic steady state is reached soon after the first cycle. The unit may be charged and discharged up to three times a day with a discharge time greater than the charge time. From a practical point of view, this is convenient since the peak periods for the energy consumption occur twice a day, in the morning and in the evening with a duration of 4–7 h. Thus, the unit may be charged during the night to be discharged the next morning and charged again in the afternoon to be discharged in the evening. The average charge and discharge times for the horizontal and vertical units are $t_c = 2.35$ h and $t_d = 4.2$ h for $NTU = 0.4$; and $t_c = 2.04$ h and $t_d = 5.92$ h for $NTU = 4$. The average discharge power of the unit is 250 W m^{-2} for $NTU = 0.4$ and 180 W m^{-2} for $NTU = 4$.

Figure 10 shows the effect of the supplied electrical power (E) on the charge and discharge times for $l = 0.02$ m. The spacing l_0 and the plate emissivities are fixed at 0.01 m and 1, respectively. The discharge time is insensitive to the supplied power variations, due to the fact that the supplied power does not affect substantially the thermal field in the PCM, and consequently, the sensible heat stored in the PCM mass will not increase significantly. However, the supplied power has a great impact on the charge time. The charge cycle will not be achieved unless the supplied power exceeds a certain value (E_0). This value corresponds in fact to the steady state regime for which the supplied power equals the discharge power

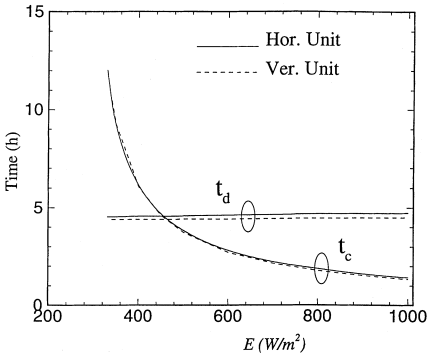

Fig. 10. Profiles of the charge and discharge times as a function of the supplied electrical power for $NTU = 1$, $l = 0.02$ m, $l_0 = 0.01$ m and $\varepsilon_{P1} = \varepsilon_{P2} = \varepsilon^i_{P3} = \varepsilon^e_{P3} = 1$.

and the temperature of plate P2 tends asymptotically to the higher set point temperature T_{high}. This threshold is given by the following formulae:

$$E_0 = \frac{\bar{T}_P - T_a}{h_t + h_{ri}} \{h_e(h_{ci} + 2h_{ri}) + h_{ci}(h_t + h_{ci} + 3h_{ri})(1 - e^{-NTU})/NTU\} \quad (26)$$

where the coefficients h_{ri} and h_e are evaluated at T_{high}. Three cases emerge. The first case corresponds to $E < E_0$; the charge cycle will never be achieved. The second case is for $E \to E_0$; the charge cycle is asymptotically achieved and the discharge cycle never starts. Finally, when $E > E_0$; both charge and discharge cycles are achieved. The value of E_0 is independent of the PCM thickness (l). It depends, however, on the higher set point temperature (T_{high}), the heat transfer coefficients (h_{ri}, h_{ci}, h_e), the number NTU and the ambient temperature T_a.

Figure 11 shows the effect of the PCM thickness (l) on the charge and discharge times for a supplied power of 700 W m^{-2}. The spacing l_0 and the plate emissivities are fixed at 0.01 m and 1, respectively. The charge and discharge times increase as the PCM thickness increases

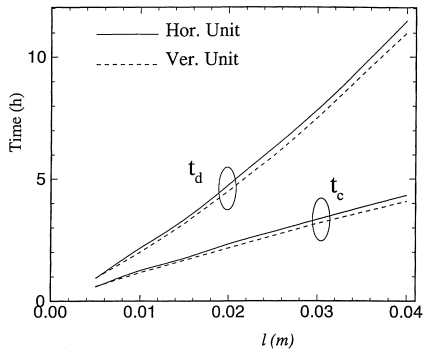

Fig. 11. Profiles of the charge and discharge times as a function of the PCM thickness for $NTU = 1$, $E = 700$ W m^{-2}, $l_0 = 0.01$ m and $\varepsilon_{P1} = \varepsilon_{P2} = \varepsilon^i_{P3} = \varepsilon^e_{P3} = 1$.

with the charge time being lower than the discharge time. The vertical unit has shorter charge and discharge times, due to free convection in the melt and more intense ambient air motion in its vicinity.

Figure 12 shows the profiles of the charge and discharge times as a function of *NTU* for different values of the spacing l_0 and different interior plate emissivities. The unit is the horizontal position with an outside surface emissivity $\varepsilon^{e}_{P3} = 1$. The charge time is practically constant except for low values of *NTU*. However, the discharge time increases substantially with the increase in *NTU* and l_0 and with a decrease in the plate emissivities. As *NTU* takes on larger values, the discharge time tends to a constant value. For this case, the unit discharges its heat essentially through plate P3 and the ventilating air exits at the average temperature $\bar{T}_P$.

6.1. *Charge and discharge time estimation*

The foregoing figures have shown that the charge time is basically a function of the supplied power (E) and that of the PCM thickness (l) while the discharge time varies mainly according to the PCM thickness l. The vertical and horizontal units have different charge and discharge times. A parameter that may indicate the position of the unit is the threshold E_0. Based on the data plotted in the Figs 11–12, one can postulate the following functions:

$$t_c = c/E_0 \cdot \frac{l^n}{(E/E_0)^a(E/E_0-1)^b}; \quad t_d = d/E_0 \cdot l^m \tag{27}$$

The constants a and b may be determined by fitting the data of Fig. 11 using the least square method, and the constant n and m by fitting the data of Fig. 12. Several values of *NTU*, ranging from 0.1–2, are used to establish global constant values. The constants are found to be $a = 1.465$, $b = 0.148$, $n = 0.943$ and $m = 1.267$.

To determine the constants c and d, the charge and discharge time equations [equations (27)] are plotted in Figs 13 and 14 for the horizontal and vertical units and for *NTU* values equal to 0.1, 1 and 2. The constants are found to be $c = 88\,670$ and $d = 216\,343$. The units in equations (27) are: l (m), E (W m^{-2}) and t (h). The maximum residual in Figs 13 and 14 are less than 15%, except at very small values of l and E. These figures provide useful information for the design of planar latent heat storage units.

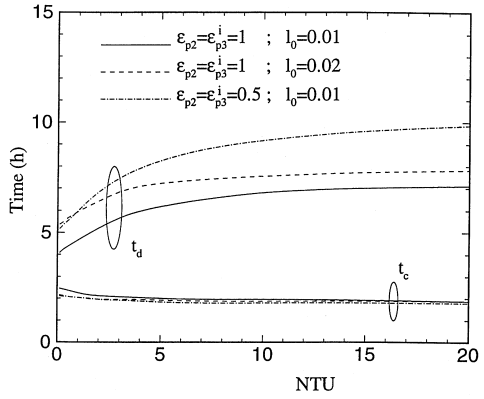

Fig. 12. Profiles of the charge and discharge times as a function of *NTU*, the spacing l_0 and the plate emissivities for $E = 700$ W m^{-2}, $l = 0.02$ m and $\varepsilon^{e}_{P3} = 1$ (horizontal unit).

7. Conclusion

A theoretical study was conducted to assess the thermal performance of a ventilated panel heating unit with latent heat storage. This unit may be used to shift the electrical load from on-peak hours to off-peak hours while it delivers sufficient heating power to the living space during charge and discharge periods. The parameters that govern the heat transfer to the living space are the supplied power (E), the PCM thickness (l), the radiation coefficients (h_{re}, h_{ri}), the convection coefficients (h_{ce}, h_{ci}), the ambient temperature (T_a) and the number of thermal units (*NTU*). The analysis showed that cyclic charges and discharges will not be achieved unless the supplied power exceeds a certain value (E_0), which is independent of the PCM thickness. The temperature of the plate in contact with the ambient air may be readily controlled and made comfortable to the occupants by choosing an appropriate value of *NTU* with respect to a threshold NTU_0. The ventilating air may exit from the unit at temperatures higher or lower than the temperature of the plate in contact with the ambient air. PCMs with high melting temperatures may, thus, be used.

The results showed that periodic steady state regime is reached soon after the first cycle of consecutive charge and discharge. The unit may be charged and discharged more than twice a day with the discharge time higher than the charge time. This is convenient, since the peak hours occur twice a day, in the morning and in the evening. The unit may be designed to be charged during the night and during the afternoon in order to be discharged during the morning and during the evening, respectively. The charge time is mainly controlled by the power supplied and the PCM thickness. Large supplied powers decrease the charge time while large PCM thicknesses do the inverse. The other parameters have less impact on the charge time. While the discharge time is nearly insensitive to the power supplied, it is strongly influenced by the PCM thickness, the radiation and convection coefficients and the *NTU* number. Large values of PCM thickness, convection coefficients and *NTU*, or low values of radiation coefficients increase substantially the discharge time. The average charge time of the unit varies between 2 and 2.4 h, and the average discharge time varies between 4 and 6 h. The unit may deliver a

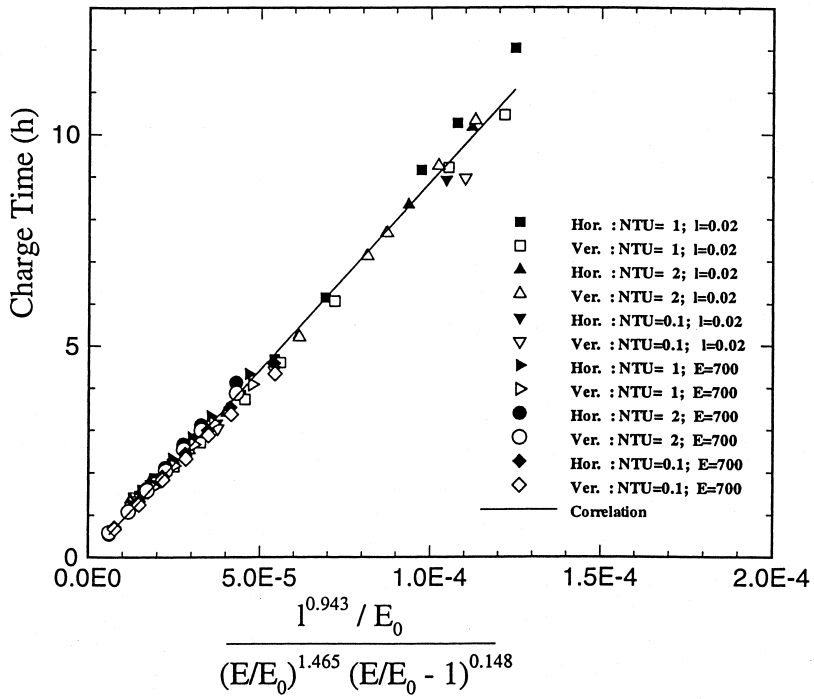

Fig. 13. Correlation curve for the charge time for $l_0 = 0.01$ m and $\varepsilon_{P2} = \varepsilon^{i}_{P3} = \varepsilon^{e}_{P3} = 1$.

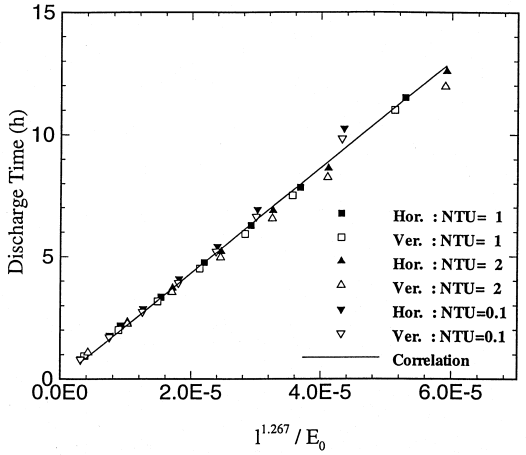

Fig. 14. Correlation curve for the discharge time for $E = 700$ W m^{-2}, $l_0 = 0.01$ m and $\varepsilon_{P2} = \varepsilon^{i}_{P3} = \varepsilon^{e}_{P3} = 1$.

heating power between 250 W m^{-2} and 180 W m^{-2}. Correlations of the charge and discharge times were established, covering the horizontal and vertical positions of the unit for a wide range of design and operating parameters.

Acknowledgements

The authors gratefully acknowledge the financial support of the 'Ministère de l'énergie et des ressources du Québec' and the 'Natural Sciences and Engineering Research Council of Canada'.

References

[1] N. Shumsundar, R. Srinivasan, Effectiveness–*NTU* charts for heat recovery from latent heat storage units, J. Solar Energy Eng. 102 (1980) 263–271.
[2] E.M. Sparrow, J.A. Broadbent, Inward melting in a vertical tube which allows free expansion of the phase-change medium, J. Heat Transfer 104 (1982) 309–315.
[3] M. Yanadori, T. Masuda, Heat transferential study on a heat storage container with phase change material, Solar Energy 36 (2) (1986) 169–177.
[4] M.M. Farid, A. Kanzawa, Thermal performance of a heat storage module using PCM's with different melting temperatures: mathematical modeling, J. Solar Energy Eng. 111 (1989) 152–157.
[5] M.M. Farid, Y. Kim, A. Kanzawa, Thermal performance of a heat storage module using PCM's with different melting temperatures: experimental, J. Solar Energy Eng 112 (1990) 125–131.
[6] M. Sozen, K. Vafai, L. Kennedy, Thermal charging and discharging of sensible and latent heat storage packed beds, J. Thermophysics 5 (4) (1991) 623–625.
[7] H.E.S. Fath, Heat exchanger performance of latent heat thermal energy storage system, Energy Conves. Mgmt 31 (2) (1991) 149–155.
[8] M. Lacroix, Numerical simulation of a shell-and-tube latent

heat thermal energy storage unit, Solar Energy 50 (4) (1993) 357–367.
[9] Y. Cao, A. Faghri, Performance characteristics of a thermal energy storage module: a transient PCM/forced convection conjugate analysis, Int. J. Heat Mass Transfer 34 (1) (1991) 93–101.
[10] Y. Cao, A. Faghri, A study of thermal energy storage system with conjugate turbulent forced convection, ASME J. Heat Transfer, 114 (1) (1992) 1019–1027.
[11] C. Bellicci, M. Conti, Phase change thermal storage: transient behaviour analysis of a solar receiver/storage module using the enthalpy method, Int. J. Heat Mass Transfer 36 (8) (1993) 2157–2163.
[12] C. Bellicci, M. Conti, Phase change thermal storage: transient behaviour analysis of a latent heat thermal storage module, Int. J. Heat Mass Transfer 36 (15) (1993) 3851–3857.
[13] Y. Zhang, A. Faghri, Semi-analytical solution of thermal energy storage system with conjugate laminar forced convection, Int. J. Heat Mass Transfer 39 (4) (1996) 717–724.
[14] B. Kalhori, S. Ramadhyani, Studies on heat transfer from a vertical cylinder, with or without fins, embedded in a solid phase change medium, J. Heat Transfer 107 (1985) 44–51.
[15] V.G. Jariwala, A.S. Mujumdar, M.E. Weber, The periodic steady state for cyclic energy storage in paraffin wax, The Canadian Journal of Chemical Engineering 65 (1987) 899–906.
[16] M. Hasan, A.S. Mujumdar, M.E. Weber, Cyclic melting and freezing, Chemical Eng. Science 46 (7) (1991) 1573–1587.
[17] Z.X. Gong, A.S. Mujumdar, Enhancement of energy charge-discharge rates in composite slabs of different phase change materials, Int. J. Heat Mass Transfer 39 (4) (1996) 725–733.
[18] M.M. Farid, R.M. Husian, An electrical storage heater using the phase change method of heat storage, Energy Convers. Mgmt. 30 (3) (1990) 219–230.
[19] A. Laouadi, Transfert de chaleur dans un matériau à changement de phase: application au stockage cyclique d'énergie électrique, Ph.D. thesis, Université de Sherbrooke, Québec, 1996.
[20] A. Laouadi, M. Lacroix, N. Galanis, A numerical method for the treatment of discontinuous thermal conductivity in phase change problems, Int. J. Numerical Methods for Heat and Fluid Flow, 1998, in press.
[21] T. Hirata, K. Nishida, An analysis of heat transfer using equivalent thermal conductivity of the liquid phase during melting inside an isothermally heated horizontal cylinder, Int. J. Heat Mass Transfer 32 (9) (1989) 1663–1670.
[22] A. Abhat, Low temperature latent heat thermal energy storage: heat storage materials, Solar Energy 30 (4) (1983) 313–332.
[23] R.K. Shah, M.S. Bhatti, Laminar convective heat transfer in ducts, in: S. Kakac, R.K. Shah, W. Aung (Eds.), Handbook of Single-Phase Convective Heat Transfer, Wiley, New York, 1987, Chap. 3.
[24] F.P. Incropera, D.P. DeWitt, Fundamentals of Heat and Mass Transfers, 4th ed., Wiley, New York, 1990.